ISSN 1063-7826, Semiconductors, 2019, Vol. 53, No. 4, pp. 411–414. © Pleiades Publishing, Ltd., 2019.
Russian Text © V.I. Orlov, N.A. Yarykin, E.B. Yakimov, 2019, published in Fizika i Tekhnika Poluprovodnikov, 2019, Vol. 53, No. 4, pp. 433–436.

NONELECTRONIC PROPERTIES OF SEMICONDUCTORS (ATOMIC STRUCTURE, DIFFUSION)

Effect of Nickel and Copper Introduced at Room Temperature on the Recombination Properties of Extended Defects in Silicon

V. I. Orlov[a,b,]*, N. A. Yarykin[a], and E. B. Yakimov[a,c]

[a] *Institute of Microelectronics Technology and Ultra-High-Purity Materials, Russian Academy of Sciences, Chernogolovka, Moscow region, 142432 Russia*

[b] *Institute of Solid-State Physics, Russian Academy of Sciences, Chernogolovka, Moscow region, 142432 Russia*

[c] *National University of Science and Technology "MISiS", Moscow, 119049 Russia*

**e-mail: orlov@issp.ac.ru*

Received November 13, 2018; revised November 20, 2018; accepted November 20, 2018

Abstract—The change in the recombination properties of individual dislocations and dislocation trails in silicon due to the diffusion of nickel and copper during chemical-mechanical polishing at room temperature is studied by the electron-beam- and light-beam-induced current techniques. It is found that the introduction of nickel results in an increase in the recombination activity of both dislocations and dislocation trails. The introduction of copper does not induce any substantial change in the contrast of extended defects.

DOI: 10.1134/S1063782619040225

1. INTRODUCTION

It is known that dislocations can greatly influence the electrical properties of silicon [1, 2]. Over the last few years, this subject matter has undergone development, since multicrystalline silicon wafers used for the production of solar cells contain a high dislocation density. Dislocations are generated by thermal strains produced upon the cooling of ingots and various technological operations of the formation of photoelectric structures. In silicon, dislocations moving at intermediate temperatures form quasi-two-dimensional extended defects in the glide plane [3, 4]. These defects, known as dislocation trails (DTs), as well as dislocations themselves, exhibit electrical activity and can be detected by the electron-beam-induced current (EBIC) and light-beam-induced current (LBIC) techniques [4–9].

Despite long-standing investigations, the nature of the electrical activity of DTs, as well as dislocations, remains a topic of discussion. The electrical activity can be determined by both the specific configuration of silicon atoms (intrinsic activity) and the decoration of structural defects by impurities. Unambiguous proof of the intrinsic nature of electrical activity has not been obtained for dislocations nor for DTs. At the same time, the growth of the recombination activity of dislocations because of metal contamination was shown for a number of impurities [2, 10–14]. As to DTs, the influence of metals on their recombination properties was investigated only in few studies [4, 5, 14–16]. In these studies, the impurity was introduced by diffusion at temperatures comparable to the deformation temperature, which could substantially modify the structure of defects. As the temperature of diffusion was lowered, the effect of metals on the electrical activity of defects in plastically deformed silicon became less pronounced [17], which could be due to the existence of an energy barrier that slows down reactions of metals with structural defects at lower temperatures. Another obvious cause lies in the fact that the impurity concentration may not be high enough, for example, because of the reduced solubility limit of the impurity.

The last-mentioned cause is irrelevant to copper and nickel impurities, since as shown previously, the chemical-mechanical polishing of silicon in a slurry contaminated by these impurities introduces them in concentrations that are orders of magnitude higher than their solubility limits at room temperature [18, 19]. In addition, the diffusion coefficients of these impurities are so high that they can penetrate tens and hundreds of micrometers at room temperature. In this study, this unique possibility is used to study the interaction of defects created by plastic deformation (dislocations and DTs) with copper and nickel impurities at room temperature.

2. EXPERIMENTAL

In this study, we used dislocation-free single-crystal silicon grown by the Czochralski method. The samples to be deformed were cut from commercially available p- and n-type wafers formed as $30 \times 4 \times 0.7$-mm rectangular prisms, with {100}-, {110}-, and

{110}-oriented faces (listed in order of decreasing area). Before the introduction of dislocations, the samples were chemically polished to remove uncontrollable dislocation sources. Individual dislocation half-loops were introduced from stress concentrators created at the {100} surface by indentation with a diamond indenter. The samples were deformed by four-point bending around the ⟨110⟩ axis at temperature of 600°C. At such a loading scheme, one part of the sample is subjected to compressive strains, and the other to tensile strains.

Chemical-mechanical polishing was conducted with a chemically stable unwoven polishing cloth moistened with commercially available silica suspension (density of 1.39 g cm^{-3}, particle size of ~40 nm) diluted tenfold with a 20% solution of KOH. The typical rate of material removal was 0.1–0.5 μm min^{-1}. The slurry was contaminated with metals by adding a small amount of nitric acid, in which nickel or copper were dissolved. This operation barely changed the alkaline character of the slurry (pH ~ 10). The final metal concentration was ~100 μg mL^{-1}.

The recombination properties of extended defects were studied by the EBIC or LBIC techniques. To perform EBIC and LBIC studies, we fabricated semi-transparent Schottky barriers on the samples. This was done by evaporation of thin Au and Al layers for the *n*- and *p*-type samples, respectively. The ohmic contacts were formed by rubbing AlGa paste onto the backside of the samples. The electron-beam energy (EBIC studies) was 35 keV (penetration depth ~9 μm). In the LBIC studies, we used a laser emitting at the wavelength 980 nm (penetration depth ~110 μm). The contrast was calculated by the formula $C = 1 - I_C/I_{C0}$, where I_C and I_{C0} are the currents collected by the Schottky barrier near the defect and far from it, respectively.

3. RESULTS AND DISCUSSION

Previously it was shown [20] that dislocation trails were formed only in the region swept by one of the three segments of a hexagonal dislocation half-loop, specifically, behind the 60° dislocation, in which the 90° partial dislocation is leading. For the crystallographic orientation used in this study, the DTs on the compressed side are formed behind one of the lateral segments of each dislocation half-loop. This specific lateral segment is defined by the Burgers vector of the particular dislocation, which can have one of two equally probable directions in both possible {111} glide planes. On the tensile side, the DTs are formed behind the bottom segment of the half-loop [20] and not considered in the study.

Figure 1 shows the EBIC and LBIC images of the same fragment of the compressed side of the *n*-Si sample, into which defects were introduced by making three imprints with a diamond indentor. The place of one of the imprints is marked by a circle. Before the final expansion of the half-loops, the imprints were removed by wet chemical etching. The outcrops of lateral segments of the dislocation half-loop at the surface of observation are marked with white arrows. The EBIC images of the DTs appear as long dark lines oriented along the ⟨110⟩ direction (black arrows). As noted above, the DTs are formed only behind one of the lateral segments, which can be clearly seen for the left and right half-loops in Fig. 1. At the same time, the DTs are formed on both sides of the imprint at the fragment center. This is indicative of the generation of dislocation half-loops with different Burgers vectors. Usually each imprint initiated the generation of one to five dislocation half-loops. The spread in this number most likely defines the variation in the contrast of defects formed by different imprints.

As expected, the EBIC and LBIC images are qualitatively similar (Figs. 1a, 1c), although the spatial resolution of the LBIC technique is lower because of a larger beam diameter. The main difference is defined by the fact that the light beam at the wavelength 900 nm penetrates much deeper than the electron beam. Since the glide planes of dislocations in this geometric arrangement deviate from the normal to the surface by an angle of ~35°, the larger penetration depth of the light beam makes it possible to obtain a quasi-three-dimensional image of the DTs. In particular, it can be seen that both DTs in the central part of the image in Fig. 1c are tilted to the same side: the gradually decreasing contrast on the left side corresponds to the deepened part of the DT. The contrast width ~120 μm corresponds to the depth ~180 μm.

Test chemical-mechanical polishing of the deformed sample in a nominally pure suspension shows that there are no noticeable changes in the EBIC and LBIC recombination contrasts. At the same time, contamination of the suspension with nickel results in a substantial increase in the contrast of both dislocations and DTs (Figs. 1b, 1d). In *n*-type silicon, the EBIC contrast of dislocations and DTs increases by factors of 1.5–2 and 2–5, respectively. For *p*-type silicon, the effect is more pronounced, since the EBIC contrast of dislocations after deformation is very weak and often below the sensitivity limit of EBIC measurements (~1%). After contamination with nickel, the dislocation contrast increases to ~10%, and the DT contrast becomes almost two times larger.

Thus, during chemical-mechanical polishing in a Ni-contaminated suspension at room temperature, recombination-active centers localized at dislocations and DTs are formed. It should be noted that the conditions of the formation of recombination centers upon the low-temperature introduction of nickel are drastically different from the conditions of diffusion at high temperatures (500–700°C). The electrical activity of defects after high-temperature treatment is often

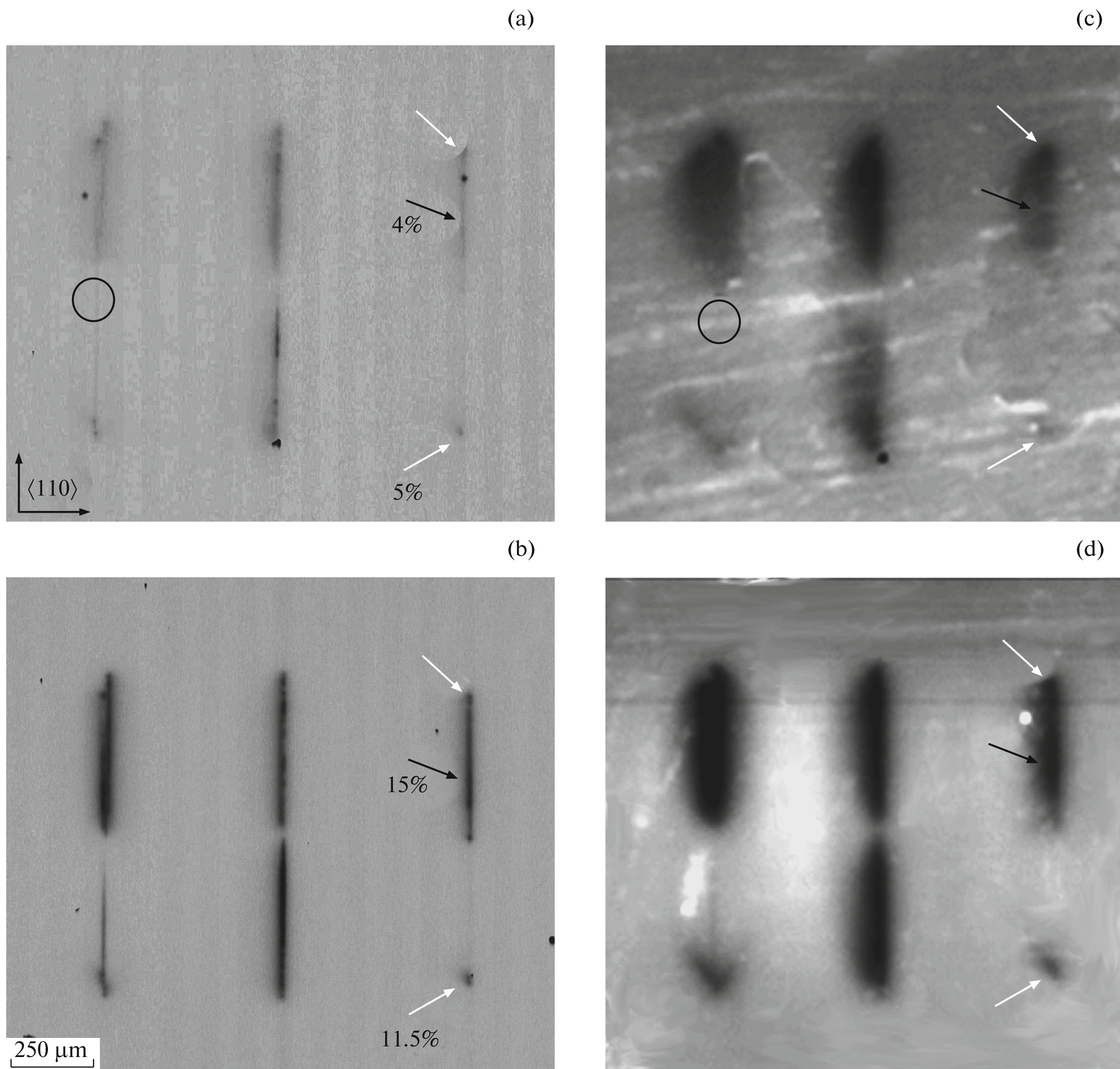

Fig. 1. (a, b) EBIC and (c, d) LBIC images of the same place at the {100} surface on the compressed side of the deformed *n*-Si sample (a, c) before and (b, d) after the introduction of nickel. White and black arrows indicate the contrasts related to dislocations and dislocation trails, respectively. The contrast values in percent are indicated. Circle marks the place of generation of the dislocation half-loop.

attributed to the formation of silicide precipitates [13], whereas growth of the second phase at temperatures close to room temperature is unlikely. The interaction of individual metal atoms with crystal imperfections is more probable; at the same time, the formation of agglomerates of rapidly diffusing impurities is possible as well. Nevertheless, of interest is a qualitative comparison of the data with the results of studies on the high-temperature introduction of metals.

The increase in the recombination contrast of dislocations because of the introduction of nickel at room temperature is consistent with previously reported data on high-temperature diffusion, although the specific mechanisms of changes in the electrical properties of dislocations in both cases remain unclear. However, the increase in the DT contrast detected here does not agree with data on the diffusion of nickel at high temperature. In [21], it was shown that the introduction of nickel at 600°C increased only the LBIC dislocation contrast, but did not increase the DT contrast. We can indicate two probable causes of this contradiction. First, in [21], nickel was introduced into samples that were annealed at 820°C after plastic deformation. The temperature 820°C is much higher

than the deformation temperature in this study. It is known [22] that the electrical properties of DTs change at a significantly lower temperature. Therefore, heat treatment at 820°C could destroy the defects, at which the nickel-related centers detected in this study are generated. Second, even if it is assumed that these precursors of recombination-active centers are rather stable, the binding energy of nickel atoms at these defects can be low, and recombination-active centers are not formed at 600°C.

As already noted above, at the crystallographic orientation under study, the contrast from DTs on the compressed side is formed only behind one of the lateral segments of the dislocation half-loop. It should be noted that a substantial increase in this contrast because of the introduction of nickel is not accompanied by the appearance of any contrast behind the opposite segment of the half-loop (right and left half-loops in Fig. 1). This observation is indirect indication of the fact that there are no “invisible” (i.e., electrically inactive) DTs behind the segment with the leading 30° partial dislocation.

In contrast to nickel, copper introduced by chemical-mechanical polishing does not induce any substantial changes in the recombination contrast of both dislocations and DTs. This is a rather unexpected result, since it was shown that, at room temperature, copper formed complexes with vacancy- and interstitial-type point defects [23–25]. Moreover, the diffusion of copper at high temperatures resulted in an increase in the contrast of DTs, although the contrast of dislocations themselves was practically unchanged in that case [15, 16].

ACKNOWLEDGMENTS

The research is carried out within the state task of IMT (no. 075-00475-19-00) and ISSP, Russian Academy of Sciences.

REFERENCES

1. W. Schroter and H. Cerva, Solid State Phenom. **85–86**, 67 (2002).
2. M. Seibt and V. V. Kveder, in *Advanced Silicon Materials for Photovoltaic Applications*, Ed. by S. Pizzini (Wiley, New York, 2012), p. 127.
3. I. E. Bondarenko, V. G. Eremenko, B. Ya. Farber, V. I. Nikitenko, and E. B. Yakimov, Phys. Status Solidi A **68**, 53 (1981).
4. I. E. Bondarenko, H. Blumtritt, J. Heydenreich, V. V. Kazmiruk, and E. B. Yakimov, Phys. Status Solidi A **95**, 173 (1986).
5. H. Alexander, S. Dietrich, M. Hühne, M. Kolbe, and G. Weber, Phys. Status Solidi A **117**, 417 (1990).
6. I. E. Bondarenko and E. B. Yakimov, Phys. Status Solidi A **122**, 121 (1990).
7. V. I. Orlov, O. V. Feklisova, and E. B. Yakimov, Semiconductors **49**, 720 (2015).
8. A. Cavallini and A. Castaldini, J. Phys., IV Colloq. **01** (C6), 89 (1991).
9. V. I. Orlov and E. B. Yakimov, Superlatt. Microstruct. **99**, 202 (2016).
10. T. S. Fell, P. R. Wilshaw, and M. D. de Coteau, Phys. Status Solidi A **138**, 695 (1993).
11. S. Kusanagi, T. Sekiguchi, B. Shen, and K. Sumino, Mater. Sci. Technol. **11**, 685 (1995).
12. M. Kittler, C. Ulhaq-Bouillet, and V. Higgs, Mater. Sci. Eng. B **24**, 48 (1994).
13. M. Seibt, V. Kveder, W. Schroter, and O. Voß, Phys. Status Solidi A **202**, 911 (2005).
14. O. V. Feklisova and E. B. Yakimov, Phys. Solid State **53**, 1240 (2011).
15. O. V. Feklisova, X. Yu, D. Yang, and E. B. Yakimov, Phys. Status Solidi C **9**, 1942 (2012).
16. O. V. Feklisova and E. B. Yakimov, Semiconductors **49**, 716 (2015).
17. M. Seibt, V. Kveder, W. Schroter, and O. Voß, Phys. Status Solidi A **202**, 911 (2005).
18. T. Zundel, J. Weber, B. Benson, P. O. Hahn, A. Schnegg, and H. Prigge, Appl. Phys. Lett. **53**, 1426 (1988).
19. N. Yarykin and J. Weber, Appl. Phys. Lett. **109**, 102101 (2016).
20. V. I. Orlov, E. B. Yakimov, and N. Yarykin, Phys. Status Solidi C **14**, 1700074 (2017).
21. V. Kveder, M. Khorosheva, and M. Seibt, Mater. Today: Proc. **5**, 14757 (2018).
22. V. G. Eremenko and E. B. Yakimov, JETP Lett. **26**, 65 (1977).
23. N. A. Yarykin and J. Weber, Semiconductors **49**, 712 (2015).
24. N. A. Yarykin and J. Weber, Semiconductors **44**, 983 (2010).
25. N. Yarykin and J. Weber, Phys. Rev. B **83**, 125207 (2011).

Translated by E. Smorgonskaya